Sensors and Materials, Vol. 38, No. 1 (2026) 127–136
MYU Tokyo

S & M 4289

Size Effects on Tensile Strength and Fracture Behavior of Carbon Nanotubes

Abbhiraj Singh,[1] Lucas Varano,[2] Masao Torii,[1]
Adam C. Powell,[2] Amit Banerjee,[1] and Takahiro Namazu[1,3*]

[1]Kyoto University of Advanced Science, 18 Yamanouchigotanda-cho, Ukyo, Kyoto 615-8577, Japan
[2]Worcester Polytechnic Institute, 100 Institute Rd, Worcester, MA, 01609, United States
[3]Tohoku University, 2-1-1 Katahira, Aoba-ku, Sendai 980-8577 Japan

(Received October 15, 2025; accepted December 24, 2025)

Keywords: Carbon nanotube, mechanical property, size effect, tensile test, strength, fracture

In this paper, the differences in mechanical properties and fracture behavior between single-walled (SW), bundled, and yarned carbon nanotubes (CNTs) are described. The three types of CNTs are subjected to a quasi-static uniaxial tensile test to investigate their Young's modulus, strength, and fracture behavior. All the samples were fractured in a brittle manner. The mean Young's modulus and strength of SWCNTs were 1 TPa and 60 GPa, respectively, which markedly decreased with increasing diameter for bundled and yarned CNTs. Fracture surface observation suggested that each type of CNT fractured in a different manner: SWCNTs were split instantly, bundled CNTs broke as the outer and inner CNTs slipped against each other, and yarned CNTs were torn apart and fractured. The differences in fracture mechanisms are discussed on basis of Raman mapping results.

1. Introduction

Carbon nanotubes (CNTs), discovered by Iijima, are the most widely studied nanocarbon materials and have attracted considerable attention across nearly all scientific and engineering communities.[1–5] Owing to their outstanding strength-to-weight ratios compared with other strong materials, single-walled CNTs (SWCNTs) are expected to be used as structural materials not only for future nanoelectronics and nanoelectromechanical devices, but also for space elevators.[6] However, all experimentally reported values are considerably lower and exhibit a considerable degree of scatter, with the lack of structural information inhibiting constraints on their associated mechanism. Even if the measured strength values are lower than the theoretical values, they are still higher than those of typical strong materials, as stated above.[7–10] If we plan to use CNTs as a mechanical engineering material, their size must be increased to at least the submillimeter scale while maintaining their high strength. However, it is a technically challenging task to increase their size without introducing defects that could lead to failure.

*Corresponding author: e-mail: namazu.takahiro@kuas.ac.jp
https://doi.org/10.18494/SAM5980

ISSN 0914-4935
https://myukk.org/

This study is conducted to compare the mechanical characteristics of SWCNTs, bundled CNTs, and yarned CNTs having diameters ranging from 1.5 nm to 100 μm, and to discuss how the superior strength of SWCNTs can be maintained even if they are enlarged to the micro or millimeter scale. Quasistatic uniaxial tensile tests are conducted using a specially developed nanoscale tensile test system featuring a microelectromechanical system (MEMS) device, as well as a microscale tensile test system utilizing commercial material evaluation equipment.[11–13] The size effects on the Young's modulus and fracture strength of various CNTs are investigated. Primarily, the fracture mechanism is examined in detail and discussed to identify strategies for maintaining the strength of several tens of GPa, not only at the nanometer scale but also at the micrometer-millimeter scale.

2. Experimental Procedure

Figure 1 illustrates the three specimen types used in the uniaxial tensile test—(a) SWCNT, (b) bundled CNT, and (c) yarned CNT—and the nano- and microscale tensile test systems. SWCNTs are synthesized by ethanol chemical vapor deposition on a Si wafer with a groove, allowing them to connect the stages on both sides, much like a bridge.[10] After the synthesis, the diameter and the number of layers are analyzed for each SWCNT using Raman and Rayleigh scattering methods.[10] The diameter of SWCNTs ranges from 1.5 to 3.0 nm. Bundled CNTs are prepared by first dispersing SWCNTs in chlorosulfonic acid and then immersing them in diazonium salt to produce phenyl bonds.[14,15] The diameter of bundled SWCNTs ranges from 15 to 100 nm. Yarned CNTs are a commercial product (Meijo Nano Carbon Co., Ltd.), prepared by spinning multiple SWCNTs. Each SWCNT is bonded solely by van der Waals forces, with no binder used. The diameter is 100 μm.

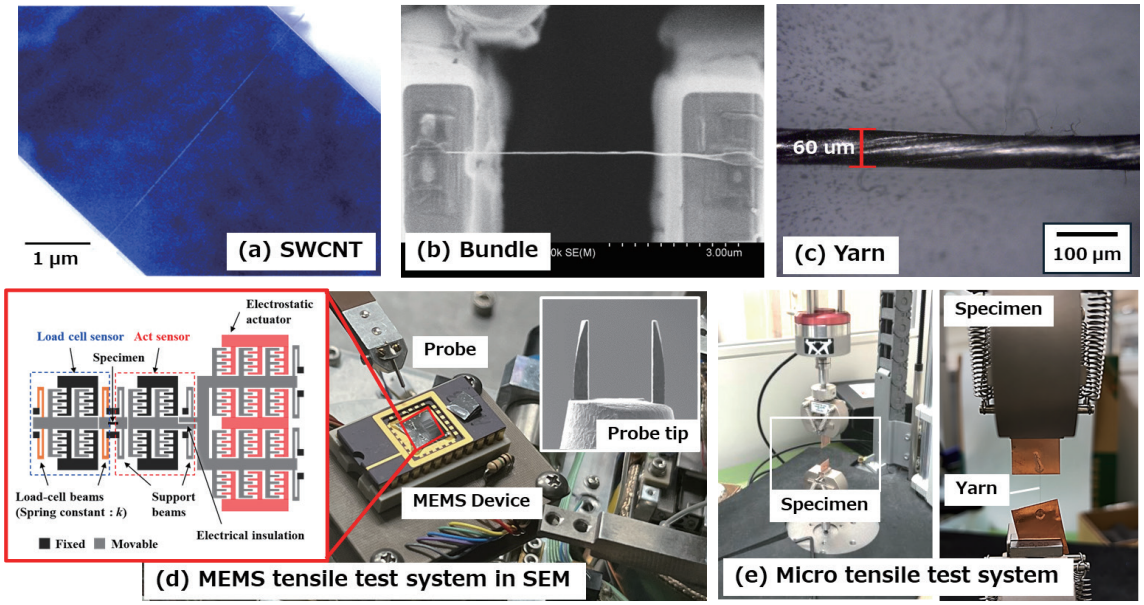

Fig. 1. (Color online) Photographs of SWCNT, bundled CNT, and yarned CNT along with the tensile test system.

SWCNTs and bundled CNTs are subjected to uniaxial tensile test using a MEMS-based nanoscale tensile test system.[10–14] The MEMS device, designed for nanowire-shaped samples, comprises an electrostatic actuator, two capacitive sensors, and a sample stage.[12] A CNT sample is picked up from the Si wafer using a probe with a twin fork [Fig. 1(d)]. The bonding between the CNT and the fork is performed using the electron-beam-induced deposition (EBID) technique.[10] Carbon contamination works like glue. Then, the picked CNT is moved to the MEMS sample stage and bonded using the EBID technique. Uniaxial tensile force is applied to the CNT via electrostatic actuators, which are actuated at 0.2 V/s until a displacement of 14 μm, for smooth quasi-static tensile loading.[12] The stage displacement and the voltage applied to the actuators have a nonlinear relationship. Therefore, the displacement speed of the stage increases linearly with the actuation voltage, which is given by the following equation:

$$\dot{x} = \frac{n_{act}\varepsilon_0 t}{k}\left\{\frac{w}{(l_0 - l_1)^2} + \frac{1}{g}\right\} 2V_{act}(t)\dot{V}_{act}, \tag{1}$$

where n_{act} is the number of comb structures, ε_0 is the dielectric constant in vacuum, $V_{act}(t)$ is the bias voltage across the actuator terminals at any instant of time t, k is the overall stiffness of the system, w is the comb finger width, g is the length of gap between the combs, l_0 and l_1 are the comb finger and overlapped lengths, respectively. The displacement speed increases by 0.0015 μm/s for a unit increment in actuation voltage. The tensile force and sample elongation are measured using the load-cell side sensor and the difference between the two capacitive sensors, respectively. They are also determined by SEM image analysis.

The mechanical strength of CNT yarns is evaluated using a universal tensile test machine (Instron Japan, ElectroPlus). Each end of a CNT yarn is fixed to a copper lamina using a commercial adhesive (Alteco CN4 Instant Glue), and the assembly is dried in a controlled laboratory environment for 24 h to ensure strong adhesion. The copper lamina helps clamp the CNT yarn sample between the jigs of the tensile test system [Fig. 1(e)]. Tensile tests are conducted at a crosshead speed of 1 mm/min until fracture. Force and sample elongation values are drawn directly from the load cell and displacement sensor of the test machine. The lengths of the SWCNT and bundled CNT were determined from the distance between the two sample stages of the MEMS device, which was 5 μm. The length of CNT yarns was aimed at 15 mm, but there were individual differences. It was measured one by one and then subjected to tensile loading. MEMS-based tensile tests are conducted in an SEM (~10^{-4} Pa) device, while micro tensile tests are carried out in a controlled laboratory environment.

3. Results and Discussion

Figure 2 shows the representative tensile stress–strain relationship of the SWCNT, bundled CNT, and yarned CNT, which are expressed as blue, red, and green colors, respectively. The numbers of samples tested were 8, 3, and 7 for the SWCNT, bundled CNT, and yarned CNT, respectively. All stress–strain curves are linear until failure, indicating that the samples failed in a brittle manner. The elongation of the samples tested in the SEM device is measured by

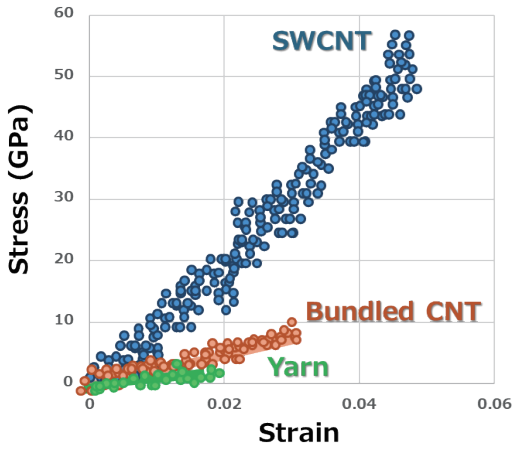

Fig. 2. (Color online) Representative tensile stress–strain relationship obtained from quasistatic tensile testing.

analyzing the images recorded during tensile tests. However, SEM images are affected by electronic noise arising from stage actuation, which introduces scatter into the detected marker positions.[10] Images of SWCNTs, with a diameter of 1.6 nm, are recorded at higher magnification than those of bundled CNTs, resulting in greater image noise and, consequently, larger data scatter.

Figures 3(a) and 3(b) show the variations in apparent Young's modulus and tensile strength as functions of CNT diameter. The color definitions for the plots used here are identical to those in Fig. 2. As shown in Fig. 3(a), the apparent Young's modulus of SWCNTs was approximately 1 TPa on average, almost the same as that of diamond[15]. Upon increasing the diameter of the samples from 10 nm to 100 nm by producing a bundle configuration ranging, the modulus decreased to 85–200 GPa, which is one-fifth to one-twentieth of the SWCNT value. Upon increasing the diameter of the samples further by producing a yarn configuration, Young's modulus in the range of 10.2–80 GPa was obtained. As compared with SWCNTs, a large scatter in Young's modulus was seen for both bundled and yarned CNTs, which implies that an individual difference in adhesion between CNTs might have appeared in those enlargement processes. At the tensile strength shown in Fig. 3(b), a similar tendency in the diameter effect is observed at Young's modulus. The strength values of SWCNTs range from 20 to 66 GPa. The theoretical strength of SWCNTs is considered to be 100–150 GPa on the basis of molecular dynamics simulation results.[16,17] This implies that some defects that the optical analyses could not detect were introduced into the SWCNT samples during the procedure we performed. However, the experimentally obtained strength values are significantly higher—by at least one order of magnitude—than those of typically strong materials[10]. By producing bundled CNTs to enhance the sample size, the strength values dropped to 1.1–10 GPa. For yarn CNTs, the value ranged from 0.6 to 1.1 GPa. The relationship between the size of CNT samples (d in nm) and their tensile strength (σ in GPa) could be fitted using a decay function [as shown by the solid line in Fig. 3(b)], which is expressed by the following equation:

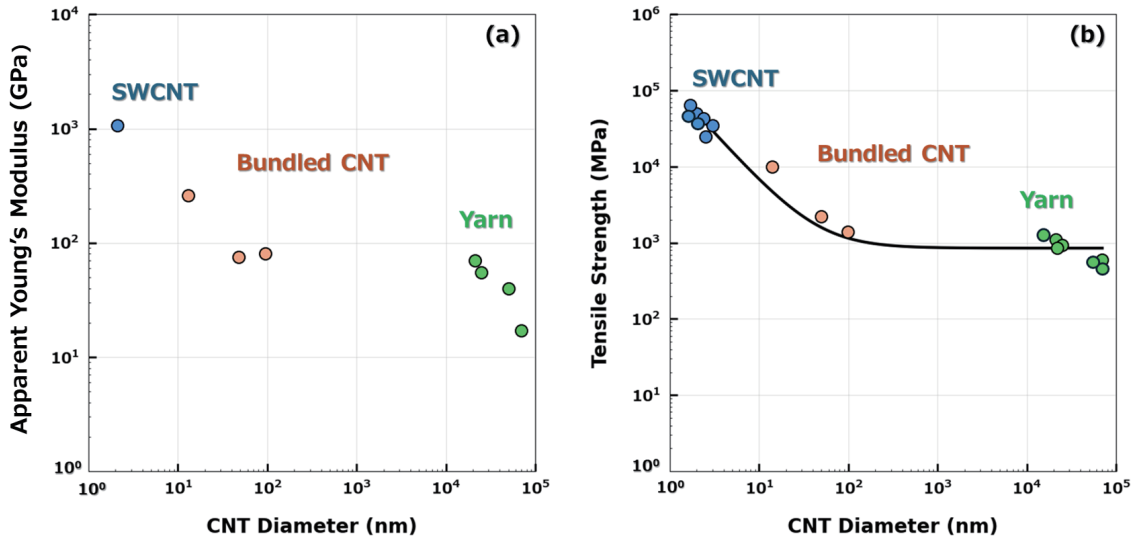

Fig. 3. (Color online) Apparent Young's modulus and tensile strength vs. CNT diameter.

$$\sigma = 0.85 + 121 d^{-1.30}. \tag{2}$$

A significant size effect phenomenon was observed in both mechanical properties in this study.

To understand why the size effect on strength is observed, the fracture mechanisms for each type of CNT are discussed. Figure 4 shows representative SEM images of fractured samples. On the basis of the snapshot of the SWCNT fracture shown in Fig. 4(a), the sample failed utterly at the center. This is because the SWCNT sample consisted of a SW tube. Once a crack was introduced to the sample, a catastrophic fracture occurred immediately.[10] In the bundled CNT shown in Fig. 4(b), however, a unique fracture different from the SWCNT fractrure was observed, where the sample fractured on the left side. In the magnified view of area A, as shown in Fig. 4(c), the diameter of the failed sample on the left side was found to be smaller than that on the right side. This bundled CNT sample was produced with dispersion and phenyl processes. After dispersion, the diazonium salt gradually penetrates the bundled CNTs from their surfaces. If the diameter of the bundled CNT is large, the salt would have penetrated only halfway, resulting in the formation of double layers with and without phenyl linkages. Therefore, the inner-bundled CNT on the left side would have separated from the outer-bundled CNT on the right side by slipping through.[14] In Fig. 4(d), the yarned CNT exhibited complex failure, with multiple small bundles of CNTs breaking off in a manner that resulted in overall fraying. The fraying phenomenon can be observed not only at the fracture point but also throughout the entire sample. The magnified view of area B shown in Fig. 4(e) suggests that the fracture occurred in a manner that caused the tip to split into multiple small fragments, implying that the interfaces between the bundled CNTs were weak. The tip of one fragment with a diameter of around 400

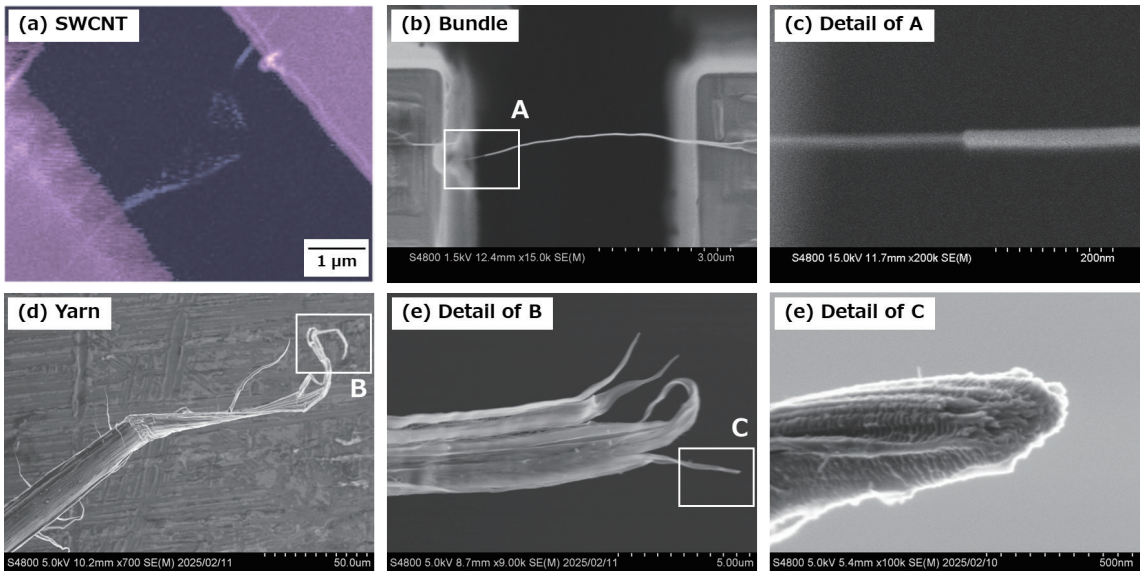

Fig. 4. (Color online) Photographs of fractured samples after quasistatic uniaxial tensile testing.

nm in the magnified view of area C, as shown in Fig. 4(f), seems to comprise multiple bundles of CNTs with a diameter of less than 50 nm. Each bundle appears to be tightly bonded to the others, even if it was bonded using the van der Waals force only, although the strength of yarned CNTs was lowest.

To facilitate deeper discussion and estimate the fracture mechanisms, Raman spectroscopic analysis was conducted. The typical Raman spectrum consisted of two peaks at 1350 and 1585 cm^{-1}, corresponding to the D- and G-bands, respectively.[18] The Raman signal intensity of the G-band peak was higher than that of the D-band peak, although the spectral data are not provided here. Thus, the G-band peak was used to map Raman spectral parameters—intensity, peak shift, and full width at half maximum (FWHM)—across the entire sample.[19]

Figure 5 shows the representative maps of the spectral parameters for bundled and yarned CNTs. Here, the data for SWCNTs are not shown because no meaningful data were obtained owing to the very small sample size. The bundled CNT was subjected to uniaxial tensile loading until fracture to determine the sample's weakest point. The red-colored part indicates the fractured point of the sample specified by the test. The intensity and Raman shift were found to be uniformly distributed across the bundled CNT sample. This suggests that the two Raman spectral parameters are not directly related to the defects that cause fracture. In contrast, the peak width is distributed nonuniformly, where the portion showing the larger peak width can be observed on the left side of the fractured point. A large Raman peak width for CNTs is known to be attributed to the defects contained within the portion.[15,19] In our previous study, the large peak width of the as-prepared bundled CNT was nearly the same as that at the fractured point, indicating that the sample fractured at the defects present there.[19] In the case of the bundled CNT sample prepared through the dispersion and phenyl processes, such defects were possibly repaired by forming phenyl bond linkages. Consequently, stress was probably concentrated at the boundary between the repaired portion and the less-defected portion during the tensile

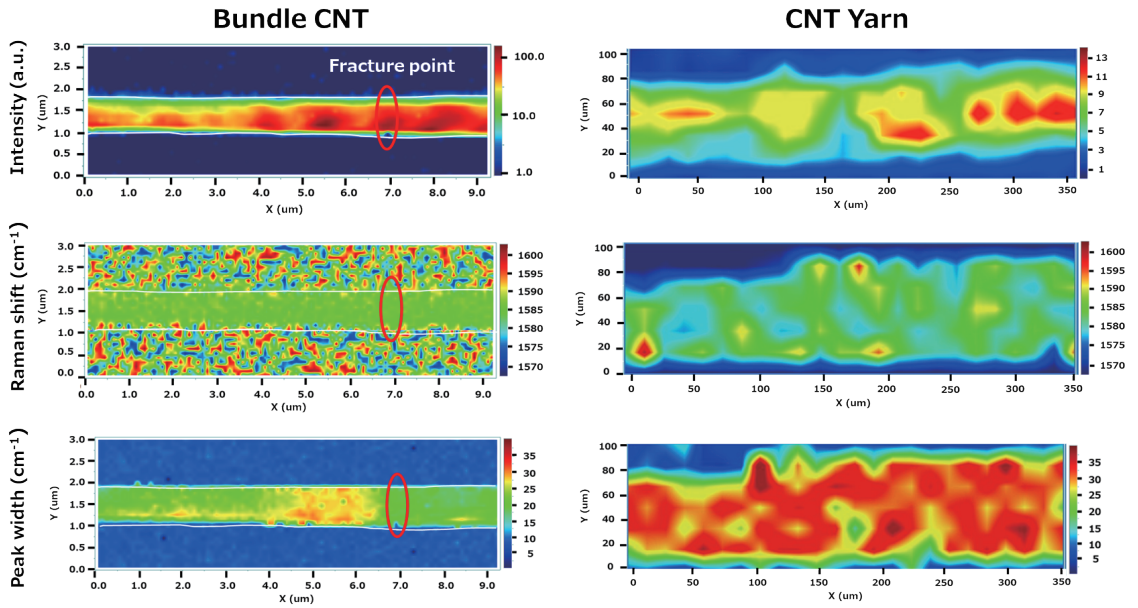

Fig. 5. (Color online) Raman intensity, peak shift, and peak width maps for bundled and yarned CNTs.

loading, so that the sample would have fractured in the vicinity of the large peak width area detected by Raman mapping. On the other hand, the yarned CNT exhibits similar trends in the intensity and Raman shift distributions, although some data scatters are observed. The scatter is attributed to the structural nonuniformity of the yarned CNT. Note that the peak width distribution for the yarned CNT differs completely from that for the bundled CNT. The former shows a uniform distribution in peak width, whereas the latter shows a nonuniform distribution. As discussed above, if the larger peak width is directly associated with the existence of defects, even for the yarned CNT, then many defects are probably included in the yarned CNT. This matches the fracture phenomenon, allowing the sample to split at any point, as observed in Figs. 4(d)–4(f). On the basis of the experimental results obtained here, it is likely that more defects are introduced during the enlargement process in CNT samples with larger diameters. Increasing the diameter while minimizing the introduction of new defects is crucial for synthesizing CNTs as engineering materials that exhibit high strength despite their large size.

4. Conclusions

In this study, the mechanical properties and fracture mechanisms of SWCNTs, bundled CNTs, and yarned CNTs were compared through quasistatic uniaxial tensile testing. Linear stress–strain relationships were obtained, indicating that brittle fracture occurred in all the tested samples. The apparent Young's modulus and tensile strength of SWCNTs were 1 TPa and 60 GPa on average, respectively, which markedly decreased to around 10 and 0.6 GPa with increasing diameter, as observed in the bundled and yarned CNTs. SEM observations revealed that the fracture mechanisms differed significantly among the three sample types. Raman

mapping suggested that the distribution of defects affected fracture and strength. The FWHM map for the G-peak of the Raman signal showed that, while bundled CNTs have defects concentrated at specific locations, the number of defects increases significantly during the enlargement process to produce yarns, thereby reducing mechanical strength. Therefore, suppressing the production of new defects in CNTs is crucial for using strong, enlarged CNTs as an engineering material.

References

1 S. Iijima: Nature **354** (1991) 56. https://doi.org/10.1038/354056a0
2 L. Qu, L. Dai, M. Stone, Z. Xia, Z. L. Wang: Science **322** (2008) 238. https://doi.org/10.1126/science.1159503
3 T. W. Odom, J. L. Huang, P. Kim, and C. M. Lieber: Nature **391** (1998) 62. https://doi.org/10.1038/34145
4 S. J. Tans, M. H. Devoret, H. Dai, A. Thess, R. E. Smalley, L. J. Geerlings, and C. Dekker: Nature **386** (1997) 474. https://doi.org/10.1038/386474a0
5 J. P. Lu: Phys. Rev. Lett. **74** (1995) 1123. https://doi.org/10.1103/PhysRevLett.74.1123
6 A. Nixon, J. Knapman, and D. H. Wright: Acta Astronautica **210** (2023) 483. https://doi.org/10.1016/j.actaastro.2023.04.008
7 M. F. Yu, B. S. Files, S. Arepalli, and R. S. Ruoff: Phys. Rev. Lett. **84** (2000) 5552. https://doi.org/10.1103/PhysRevLett.84.5552
8 M. F. Yu, O. Lourie, M. J. Dyer, K. Moloni, T. F. Kelly, and R. S. Ruoff: Science **287** (2000) 637. https://doi.org/10.1126/science.287.5453.637
9 M. S. Wang, D. Golberg, and Y. Bando: Adv. Mater. **22** (2010) 4071. https://doi.org/10.1002/adma.201001463
10 A. Takakura, K. Beppu, T. Nishihara, A. Fukui, T. Kozeki, T. Namazu, Y. Miyauchi, and K. Itami: Nat. Commun. **10** (2019) 3040. https://doi.org/10.1038/s41467-019-10959-7
11 T. Fujii, T. Namazu, K. Sudoh, S. Sakakihara, and S. Inoue: ASME J. Eng. Mater. Technol. **135** (2013) 041002. https://doi.org/10.1115/1.4024545
12 T. Fujii, K. Sudoh, S. Inoue, and T. Namazu: Sens. Mater. **28** (2016) 89. https://doi.org/10.18494/SAM.2016.1159
13 G. Ina, T. Fujii, T. Kozeki, E. Miura, S. Inoue, and T. Namazu, Jpn. J. Appl. Phys. **56** (2017) 06GN17. https://doi.org/10.7567/JJAP.56.06GN17
14 M. Schirowski, G. Abellan, E. Nuin, J. Pampel, C. Dolle, V. Wedler, T. Fellinger, E. Spiecker, F. Hauke, and A. Hirsch: J. Am. Chem. Soc. **140** (2018) 3352. https://doi.org/10.1021/jacs.7b12910
15 R. Kobayashi, T. Kino, and T. Namazu: Proc. ATEM-iDICs 2023 (Fukui, Oct. 2023) 09-A43.
16 M. Werner, S. Hein, and E. Obermeier: Diamond Relat. Mater. **2** (1993) 939. https://doi.org/10.1016/0925-9635(93)90254-Y
17 T. Belytschko, S. P. Xiao, G. C. Schatz, and R. S. Ruoff: Phys. Rev. B **65** (2002) 235430. https://doi.org/10.1103/PhysRevB.65.235430
18 S. Zhang, S. L. Mielke, R. Khare, D. Troya, R. S. Ruoff, G. C. Schatz, and T. Belytschko: Phys. Rev. B **71** (2005) 115403. https://doi.org/10.1103/PhysRevB.71.115403
19 T. Kino and T. Namazu: Proc. MNC 2021 (Online, Oct. 2021) 29C-1-1.

About the Authors

Abbhiraj Singh received his B.E. degree in mechatronics engineering from Kyoto University of Advanced Science (KUAS), Kyoto, Japan, in 2025. He is currently pursuing a master's degree at the Nanomechatronics laboratory at KUAS under the guidance of Prof. Takahiro Namazu. His research interests include exploring piezoresistivity in Si and SiO_2 nanostructures for their development in advanced sensing applications, and identifying novel material responses observable at the nanometer scale.

Lucas Varano received his B.S. degree in mechanical engineering from Worcester Polytechnic Institute (WPI), Worcester, Massachusetts, USA, in 2025. He is currently pursuing a master's degree in mechanical engineering at WPI. His research interests include investigating the size effect on the mechanical strength of micro- and nanoscale structures and exploring the dynamics of nanoscale combustion particles.

Masao Torii received his B.E. degree in mechatronics engineering from Kyoto University of Advanced Science (KUAS), Kyoto, Japan, in 2024. He is currently pursuing a master's degree at the Nanomechatronics laboratory at KUAS. His research interests include investigating the size effect on the mechanical strength of 3D-printed resin micro- and nanostructures, as well as exploring the functions of new materials that emerge at the nanometer scale.

Adam C. Powell, IV, is an Associate Professor in the Mechanical & Materials Engineering department who joined the WPI faculty in August 2018. His field is materials processing, and his research focuses on reducing, eliminating, and drawing down greenhouse gas emissions. His current projects aim to reduce vehicle body weight, reduce or eliminate aviation greenhouse gas emissions, develop power ships and trains over thousands of km with zero emissions, and improve grid stability as we drive toward 100% renewables. The primary tools for achieving these goals are the mathematical and techno-economic modeling of metal processes, particularly electrochemical processes, validated by key experiments.

Amit Banerjee received his M.Sc. (2009) and Ph.D. (2014) degrees from the Department of Physics at the Indian Institute of Technology Kanpur, India. He subsequently worked as a researcher at the City University of Hong Kong, Kyoto University, and the Japan Advanced Institute of Science and Technology. In September 2020, he joined the Graduate School of Engineering at Kyoto University as a Junior Associate Professor. He has been working as an Associate Professor at Kyoto University of Advanced Science since May 2025. Amit Banerjee is interested in MEMS, NEMS, nanomechanics, and other emerging areas of micro- and nanoscience and technology. He is a recipient of the JSPS postdoctoral fellowship.

Takahiro Namazu received his B.S., M.S., and Ph.D. degrees in mechanical engineering from Ritsumeikan University, Kusatsu, Japan, in 1997, 1999, and 2002, respectively. From 2002 to 2006, he served as an assistant professor in the Department of Mechanical and Systems Engineering at the Graduate School of Engineering, University of Hyogo, Himeji, Japan. In 2007, he was appointed as an associate professor at the same university. In 2010, he joined the Precursory Research for Embryonic Science and Technology program of the Japan Science and Technology Agency as a researcher. In 2016, he became a professor in the Department of Mechanical Engineering at Aichi Institute of Technology, Toyota, Japan. In 2020, he became a professor in the Faculty of Engineering at KUAS. Since 2025, he has been a Professor at the International Center for Synchrotron Radiation Innovation Smart at Tohoku University, in a cross-appointed position. He is currently engaged in studies on functional film materials, such as self-propagating exothermic materials, and their applications to micro- and nano-electromechanical systems. (namazu.takahiro@kuas.ac.jp)